

Journal of Applied Remote Sensing

RemoteSensing.SPIEDigitalLibrary.org

Distortion measurement and geolocation error correction for high altitude oblique imaging using airborne cameras

Yiming Cai
Yalin Ding
Jihong Xiu
Hongwen Zhang
Chuan Qiao
Qihui Li

SPIE.

Yiming Cai, Yalin Ding, Jihong Xiu, Hongwen Zhang, Chuan Qiao, Qihui Li, "Distortion measurement and geolocation error correction for high altitude oblique imaging using airborne cameras," *J. Appl. Remote Sens.* **14**(1), 014510 (2020), doi: 10.1117/1.JRS.14.014510

Distortion measurement and geolocation error correction for high altitude oblique imaging using airborne cameras

Yiming Cai,^{a,b} Yalin Ding,^{a,*} Jihong Xiu,^a Hongwen Zhang,^a
Chuan Qiao,^c and Qihui Li^{a,b}

^aChinese Academy of Sciences, Changchun Institute of Optics,
Fine Mechanics and Physics, Changchun, China

^bUniversity of Chinese Academy of Sciences, Beijing, China

^cBeijing Institute of Control Engineering, Beijing, China

Abstract. To measure the image distortion during the actual operation of an airborne camera, improve the accuracy of geolocation using airborne cameras, and reduce the influence of image distortion on location results, a distortion measurement algorithm based on overlapping remote sensing images is proposed, which attempts to overcome the image distortion caused by external working environment. A distortion measurement algorithm based on the geographical locations of the image coincident points is presented, and the distortion rate for the camera is calculated. To correct the positioning error caused by image distortion, the coordinate values of the target projection in the charge-coupled device coordinate frame are processed based on the distortion rate. The simulation results show that positioning accuracy decreases with increase in the distortion rate. When the distortion rate is 4%, use of the correction algorithm can improve positioning accuracy by 21%. The flight test shows that the maximum distortion rate measured by the algorithm for the experimental camera is approximately 9%. After correction, positioning error is reduced by 50 to 100 m, and positioning accuracy is greatly improved to meet the needs of actual engineering. © 2020 Society of Photo-Optical Instrumentation Engineers (SPIE) [DOI: [10.1117/1.JRS.14.014510](https://doi.org/10.1117/1.JRS.14.014510)]

Keywords: airborne camera; distortion measurement; target geolocation algorithm; overlapping image; error analysis.

Paper 190680 received Sep. 3, 2019; accepted for publication Dec. 23, 2019; published online Jan. 20, 2020.

1 Introduction

With the development of high-altitude and long-distance oblique imaging airborne cameras (HLOACs), high-resolution imaging is no longer the only research focus. High-precision target geolocation is also an active research field.¹⁻¹⁷

To obtain the high-precision position information of a target, many scholars have conducted extensive research on geolocation algorithms and the reasons for geolocation errors. In the traditional geolocation algorithm, a laser rangefinder (LRF) is usually required to obtain the distance between the airborne camera and the target. However, the LRF has a limited working distance compared to HLOAC's working distance of more than 30 km. Thus, it is difficult for the usual LRF to meet the actual requirements. In recent years, scholars prefer to use the information provided by images and camera to locate targets. Stich¹ proposed a target geolocation algorithm based on the ellipsoidal earth model to achieve the passive positioning of aerial cameras corresponding to ground targets. The author's aim was to reduce the influence of the earth's curvature on target geolocation accuracy. Qiao et al.² established a geolocation algorithm based on the digital elevation model (DEM), aiming to reduce error due to the target elevation caused by the ellipsoidal earth model. However, the DEM database needed by this method is too large to be carried on the aircraft. This method cannot locate the target in real time. Research shows that

*Address all correspondence to Yalin Ding, E-mail: dingyl_1964@126.com

line of sight (LOS) error has a great influence on the positioning result. Thus, to address this problem, Bai et al.¹⁵ proposed an algorithm for locating the same target at different points by using two unmanned aerial vehicles (UAVs). Based on the precision advantages of the combination of heterogeneous sensors, Lee et al.¹⁶ proposed a cooperative positioning system based on multiple UAVs.

At present, the optimization of geolocation algorithms mainly focuses on processing LOS errors and the target elevation error,^{1,4-16} while other error factors are rarely considered. In the case of high-altitude and long-distance oblique imaging, complex and variable environments are involved that cause image distortion resulting in location errors. Scholars have conducted extensive research on the correction of lens distortion. Lee et al.¹⁸ presented a method to correct the radial distortion caused by a camera lens. Su et al.¹⁹ proposed a distortion correction method that directly uses a standard grid plate as a measurement reference. However, most of such research in the industry associated with airborne cameras is to make corrections to the camera at the ground laboratory before the actual work is conducted and to determine the distortion due to the camera parts by using standard reference objects such as grid plates.^{10,19-23} Distortion caused by the external environment is rarely considered. Thus, the location error caused by distortion remains uncorrected.

This paper proposes a method in which the distortion rate is calculated using corresponding points in the overlapping parts of different images and location information of the target points. A distortion correction model is then established on the camera coordinate system to improve the accuracy of the geolocation algorithm. The effectiveness of the two algorithms is proved via simulation analysis and actual flight test.

2 Distortion Measurement Algorithm for High-Altitude and Long-Distance Oblique Imaging Airborne Camera

2.1 Distortion Measurement Algorithm Based on Overlapping Image

2.1.1 Distortion measurement algorithm

To describe the size of the distortion variable at a certain point in the image, the concept of distortion rate is introduced, which is defined as follows:

$$D = \frac{Z - H}{H} \times 100\%, \quad (1)$$

where D is the distortion rate, Z represents the actual imaging height, and H represents the ideal imaging height.¹⁰

The swept-type HLOAC operates at a certain image overlap rate—overlap means that the image capturing area of each image partially overlaps with that of the previous image.²⁴ Taking the sweep direction as an example [x axis direction of the charge-coupled device (CCD) coordinate frame], and considering that the carrier platform is not completely stable when working, the overlap rate is usually set to 50% to ensure that three consecutive images have two parts that overlap completely (the green and yellow portions in Fig. 1).

In the figure, the two target points a and b are located at the edges of the second image and are called the edge points a_2 and b_2 . In the first and third images, they are located at the center point of the CCD frame and are called the center points a_1 and b_1 . Since the three images are continuously obtained in a very short time, the airborne camera can be considered to be in the same operating state, and the different results obtained by positioning the same target in the three remote sensing image data are only due to image distortion. To simplify the calculations, the two points present symmetrically at the image centers can be seen to have equal distortion rates.

Because there is no distortion at the image center, the maximum distortion rate D_1 of the camera sweep direction can be obtained using Eq. (2), where d_1 is the nominal distance value without distortion, calculated using the first and third images and d_2 is the actual distance value, including the errors caused by image distortion, calculated using the second image. The distance between two target points can be calculated using the coordinate values in the earth-centered

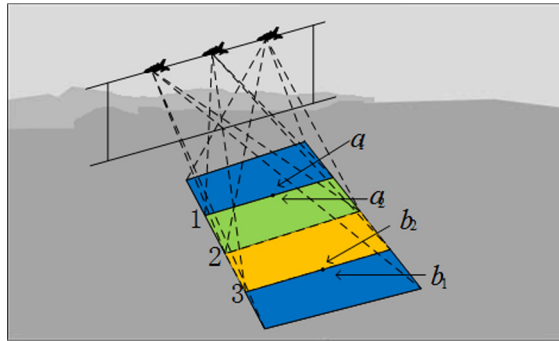


Fig. 1 Schematic representation of the results with a 50% image overlap rate.

earth-fixed (ECEF) coordinate frame, which were obtained via the geolocation algorithm described in Sec. 2.1.2.

$$D_1 = D_{\max} = \frac{d_2 - d_1}{d_1} \times 100\%. \quad (2)$$

To obtain the distortion rates for other positions, the overlap ratio of the HLOAC was adjusted, taking the image overlap ratio of 40% as an example, as shown in Fig. 2. In the figure, because a_2 and b_2 are still located at the edges of the image, their distortion rate is still D_1 . The coordinates of a_1 and b_1 on the x axis are 20% of the maximum values on the x axis, and thus, the distortion rate here is $D_{0.2}$. If the true distance between the two target points is d , then d_1 and d_2 should satisfy the following equation:

$$\begin{cases} d_1 = d \times (1 + D_{0.2}) \\ d_2 = d \times (1 + D_1) \end{cases}, \quad D_{0.2} = \frac{[D_1 - (d_2 - d_1)/d_1]}{1 + (d_2 - d_1)/d_1}. \quad (3)$$

Let $s = (d_2 - d_1)/d_1$. The equation can be abbreviated as

$$D_{0.2} = (D_1 - s)/(1 + s). \quad (4)$$

Therefore, the distortion rates of all pixel positions in the x axis direction can be obtained by adjusting the camera overlap ratio. To conveniently describe the position of a single pixel in the whole CCD, a parameter j is constructed, which refers to the ratio of the pixel position of the target projection to the maximum value of the pixel in a certain direction. For example, if the pixel of the target projection point is (560, 780), and the total number of CCD pixels is 1500×2000 , then $j_x = 0.373$, $j_y = 0.39$. The x axis distortion rate at a certain point A with coordinates (m, n) in the CCD coordinate frame can be uniformly expressed as Eq. (5):

$$\begin{cases} D_j = (D_{\max} - s)/(1 + s) \\ s = (d_{\max} - d_j)/d_j \end{cases}. \quad (5)$$

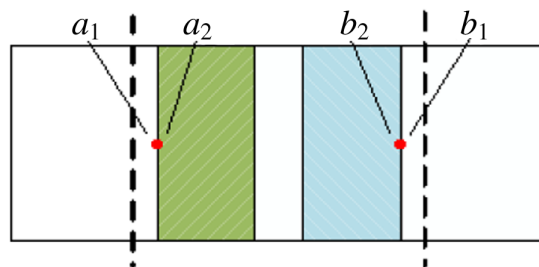


Fig. 2 Schematic representation of the results with a 40% image overlap rate.

2.1.2 Geolocation algorithm for high-altitude and long-distance oblique imaging airborne camera

In this study, the distortion measurement algorithm established requires the position information of the target point in the overlapping image, which is calculated using the target geolocation algorithm. The geolocation algorithm for HLOAC establishes a coordinate frame using various angle parameters of the aircraft and the camera and calculates the geographical location information of a target via coordinate transformation. To do this, it requires a series of coordinate frames. The position of a point in space with respect to different coordinate frames can be calculated using the transformation matrix. Here C_A^B represents the transformation matrix from frame A to frame B.

$$\begin{bmatrix} X_B \\ Y_B \\ Z_B \end{bmatrix} = \begin{bmatrix} X_A \\ Y_A \\ Z_A \end{bmatrix} \times C_A^B, \quad C_B^A = (C_A^B)^{-1}. \tag{6}$$

When the HLOAC images the ground target area, the target is projected on the CCD. The CCD coordinate frame is shown in Fig. 3. If a is the single pixel size of the camera CCD (with the focal length f), the total number of pixels is $M \times N$, and the target point is projected within the (m, n) pixel. The coordinate of the target projection point in the camera coordinate frame can be described by Eq. (7):

$$T'_C = \left[\left(m - \frac{M}{2} \right) \times a, \left(\frac{N}{2} - n \right) \times a, -f \right]^T. \tag{7}$$

Traditional positioning process is not the research focus of this paper. Thus, only the geolocation algorithm with simple formulas, such as Eqs. (6)–(9), have been described herein. The development and calculation processes of the algorithm are not discussed in detail. The relevant formulas have been extensively studied and published by scholars.^{1–17,25} A basic target geolocation process can be found in Sec. 6.

The geolocation algorithm usually requires four basic coordinate systems, namely, the ECEF coordinate frame, the geographical coordinate frame such as north–east–down (NED) coordinate frame, the aircraft coordinate frame (A), and the camera coordinate system (C). The coordinates of the target projection point in the ECEF coordinate frame can be calculated using Eq. (8):

$$T'_E = \begin{bmatrix} x'_T \\ y'_T \\ z'_T \end{bmatrix} = C_{NED}^{ECEF} \times C_{AC}^{NED} \times C_C^A \times T'_C. \tag{8}$$

The coordinate of the center of the camera optical system in the ECEF coordinate frame is $O_C = [x_C, y_C, z_C]^T$, the position of the target point in the ECEF coordinate frame $[x_T, y_T, z_T]^T$ should be on the line between the camera center and the target projection point in the ECEF

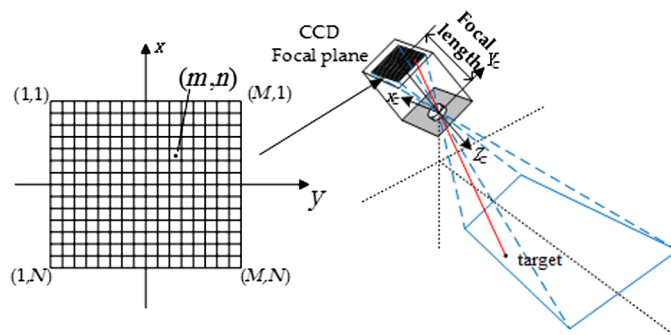


Fig. 3 Schematic representation of the HLOAC and camera coordinate.

coordinate frame. This line is established as per Eq. (9). The position of the target in the ECEF coordinate system can be obtained by solving the earth ellipsoid and linear equations.

$$\frac{x_T - x_C}{x'_T - x_C} = \frac{y_T - y_C}{y'_T - y_C} = \frac{z_T - z_C}{z'_T - z_C}. \tag{9}$$

2.2 High-Altitude and Long-Distance Oblique Imaging Airborne Camera Distortion Rate Approximation Algorithm That Uses the Stationary Overlap Rate

When an airborne camera is in operation, a situation may arise in which the overlap rate cannot be adjusted. If the camera is returned to the ground laboratory to adjust the overlap rate setting values, the working environment and posture of the aircraft will change significantly; in such a case, the effectiveness of the algorithm cannot be guaranteed. For an airborne camera with a fixed overlap rate, this paper proposes a simple and effective approximation algorithm to calculate the distortion rates of the camera.

The maximum distortion rate in a certain direction of the aerial camera can be calculated using Eq. (2). If the overlap rate of the camera is fixed, it is necessary to approximate the true distance between two points to obtain all parameters required by the algorithm. Because there is no distortion at the image center, the approximate true distance between points *a* and *b* can be calculated using the image center position.

As shown in Fig. 4, if the camera working overlap ratio is 20%, the distance between the image centers of adjacent images is 80% with respect to the entire image. For HLOAC, in the process of outward scanning or outward sweep imaging, as the frame angle increases, the shooting range for each image is larger than that for the previous image. Therefore, the corresponding parameters can be selected for correction to approximate the true distance between points *a* and *b*.

$$d = d_{1,2}/0.8 + (d_{2,3} - d_{1,2}) \times 0.2. \tag{10}$$

After many experiments, the error between the result calculated by Eq. (10) and the actual distance was obtained as less than 50 m. A 50-m error has little effect on the final calculated distortion rate. Then, using Eqs. (2)–(5) for calculation, the distortion rates D_1 and $D_{0.6}$ were obtained.

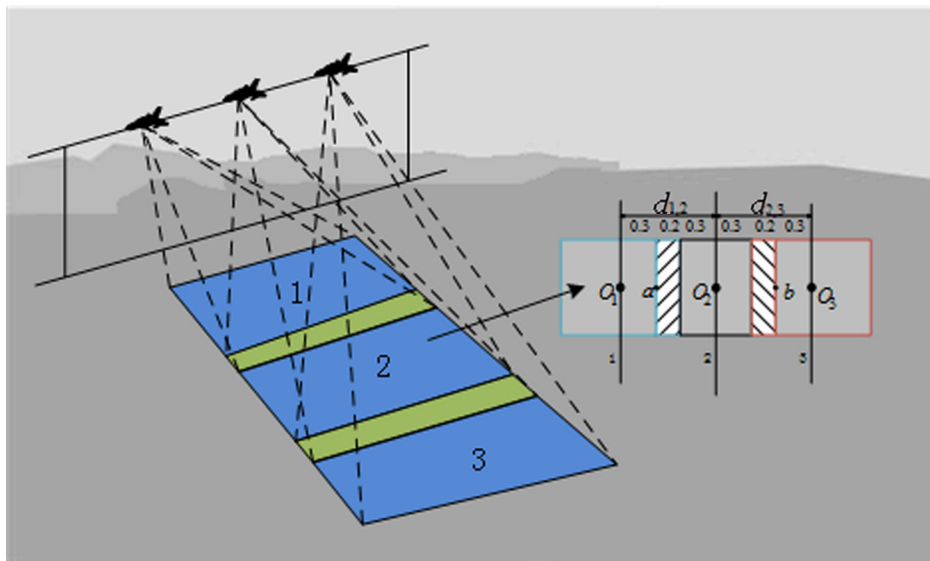


Fig. 4 Schematic representation of the results with a 20% image overlap rate.

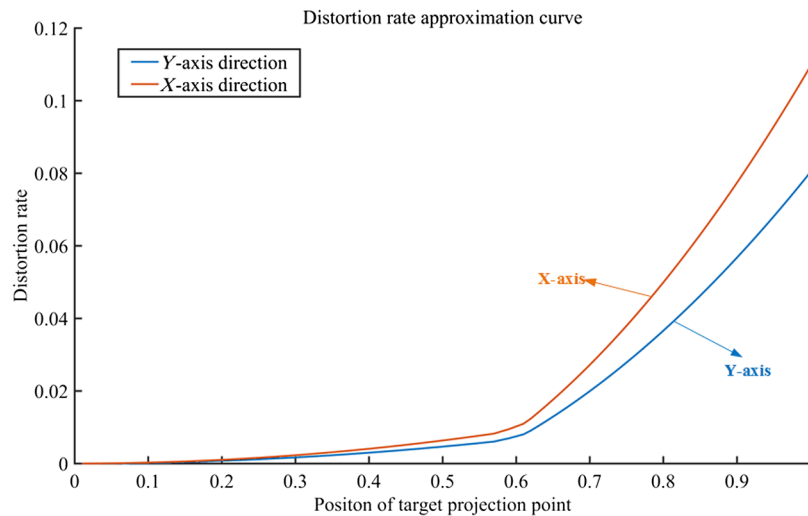


Fig. 5 Distortion rate curve.

In summary, for an HLOAC with overlap rate fixed at p , the actual distance between two points a and b at the edges of the second image can be approximately obtained using Eq. (11). The distortion rate curve is similar in shape to a conic section. Equation (12) can be used to calculate the parameters of such a curve, and the curve is drawn to approximately obtain the distortion rate of each point in the camera CCD coordinate frame. The shape of the distortion rate curve is shown in Fig. 5.

$$d = d_{1,2}/(1 - p) + (d_{2,3} - d_{1,2}) \times p, \quad (11)$$

$$\begin{cases} D_j = uj^2 + vj + c \\ j = x/x_{\max} \\ D_0 = 0 \end{cases} . \quad (12)$$

HLOAC also produces overlapping parts in the flight direction under normal conditions. The first image of each strip can be used to calculate the flight direction (y axis direction of the CCD coordinate frame) distortion rate of the camera by heading the overlap ratio. The calculation method is exactly the same as that for the sweep direction. Therefore, the distortion measurement algorithm established in this paper can calculate the distortion rate of any point on the CCD.

2.3 Correction Algorithm for Geolocation Error Caused by Distortion

To solve the positioning error caused by distortion, this paper establishes a distortion correction algorithm for application during the positioning process. With this algorithm, the projection position of a target point on the CCD coordinate frame is corrected. If the entire image is corrected for distortion, it is necessary to calculate the ideal imaging position of all the pixels, which is cumbersome to calculate. Considering that the target localization algorithm uses the coordinate values of the target point projection in the camera coordinate system for calculation, it is not necessary to perform pixel position correction on the entire distortion image. Only the ideal coordinate value of the target point needs to be calculated. According to the single pixel size of the aerial camera CCD, the ideal coordinate value of the target point projection in the camera coordinate system can be obtained by a two-step calculation. The specific steps are as follows.

First, according to the projection position of the target point on the CCD, the coordinate value (x_d, y_d) of the point on the CCD coordinate frame can be obtained as

$$x_d = \left(m - \frac{M}{2}\right) \times a, \quad y_d = \left(\frac{N}{2} - n\right) \times a. \quad (13)$$

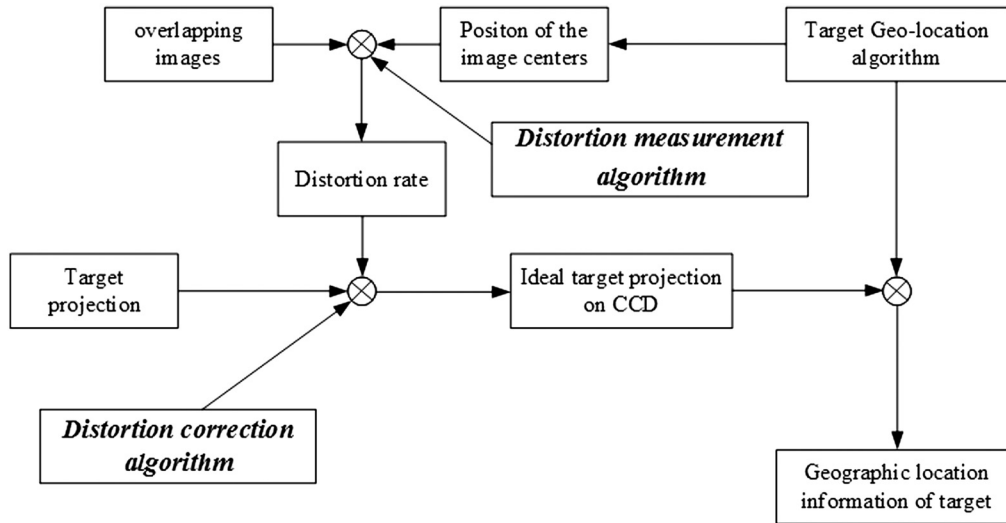


Fig. 6 Flow chart of algorithm.

Then, according to the distortion curve described in Secs. 2.1 and 2.2, the lateral and longitudinal distortion rates (D_x, D_y) corresponding to the point can be obtained, and the true projection position of the target point is calculated using Eq. (14):

$$x_r = x_d / (1 + D_x), \quad y_r = y_d / (1 + D_y). \quad (14)$$

Finally, the geographical location information of the target point is obtained using the geolocation algorithm by the corrected ideal projection position T'_{Cr} .

$$T'_{Cr} = (x_r, y_r, -f)^T. \quad (15)$$

The whole process of distortion measurement and positioning error correction is shown in Fig. 6.

3 Analysis of Positioning Error Caused by Distortion

It is necessary to simulate the geolocation algorithm before the actual flight test. The traditional simulation process generally adopts the total differential method. Because the target positioning process is calculated indirectly, it generally has the form of an elementary multivariate function, which can be expressed as Eq. (16).

$$y = f(x_1, x_2, \dots, x_n). \quad (16)$$

In Eq. (16), x_1, x_2, \dots, x_n represent direct measurement values of angle parameters in the geolocation algorithm, while y is an indirect measurement value, which represents the positioning result. For multivariate functions, the total differential of the parameter can be used to represent the increment of the function. Accordingly, the increment of the above equation is given as

$$dy = \frac{\partial f}{\partial x_1} dx_1 + \frac{\partial f}{\partial x_2} dx_2 + \dots + \frac{\partial f}{\partial x_n} dx_n. \quad (17)$$

The errors for direct measurement values can be expressed as $\Delta x_1, \Delta x_2, \dots, \Delta x_n$. These errors can be regarded as smaller values, which can be used instead of the differential components in Eq. (17):

$$\Delta y = \frac{\partial f}{\partial x_1} \Delta x_1 + \frac{\partial f}{\partial x_2} \Delta x_2 + \dots + \frac{\partial f}{\partial x_n} \Delta x_n. \quad (18)$$

The total differential method needs to divide the target positioning error into three axes in the ECEF coordinate frame. According to the mathematical model of the target positioning, the errors in the X and Y axes directions (M_X , M_Y) can be obtained.

$$M_X = \left[\left(\frac{\partial X}{\partial X_C} \delta X_s \right)^2 + \left(\frac{\partial X}{\partial Z_C} \delta Z_s \right)^2 + \left(\frac{\partial X}{\partial Z_A} \delta Z_A \right)^2 + \left(\frac{\partial X}{\partial \theta} \delta \theta \right)^2 + \left(\frac{\partial X}{\partial \gamma} \delta \gamma \right)^2 + \left(\frac{\partial X}{\partial \varphi} \delta \varphi \right)^2 \dots \right]^{\frac{1}{2}}, \quad (19)$$

$$M_Y = \left[\left(\frac{\partial Y}{\partial Y_C} \delta X_s \right)^2 + \left(\frac{\partial Y}{\partial Z_C} \delta Z_s \right)^2 + \left(\frac{\partial Y}{\partial Z_A} \delta Z_A \right)^2 + \left(\frac{\partial Y}{\partial \theta} \delta \theta \right)^2 + \left(\frac{\partial Y}{\partial \gamma} \delta \gamma \right)^2 + \left(\frac{\partial Y}{\partial \varphi} \delta \varphi \right)^2 \dots \right]^{\frac{1}{2}}. \quad (20)$$

The error in the Z axis direction is only related to the altitude, The Z axis error can, thus, be expressed as

$$M_Z = \delta H. \quad (21)$$

According to error synthesis theory, the target positioning error can be calculated using Eq. (22):

$$M = \sqrt{M_X^2 + M_Y^2 + M_Z^2}. \quad (22)$$

Although the total differential method can be used for simulation analysis, the calculation steps are too complex and time-consuming. With the development of computer technology, the Monte Carlo method is increasingly used for error analysis because its accuracy and calculation speed are better than those of the total differential method.

The Monte Carlo method can unify all kinds of random errors into one model. It only needs to select the corresponding error source for different positioning algorithms, without the divide calculation and error synthesis in the total differential method. Hence, it is widely used in fields that require many calculations in the simulation process, such as target tracking, target positioning, and remote sensing mapping. The Monte Carlo method, also called a statistical simulation method, is an approximate calculation method based on probability and statistics theory. The random error in the process of target positioning by an airborne camera usually conforms with the normal distribution; using a computer, one can easily obtain the corresponding random number sequence for simulation analysis. The error model established using the Monte Carlo method is

$$\Delta y = f(x + \Delta x_1, x_2 + \Delta x_2, \dots, x_n + \Delta x_n) - f(x_1, x_2, \dots, x_n), \quad (23)$$

where Δy is the error of the function value y and indicates the distance between the result calculated by the geolocation algorithm and the actual position of the target. Here x_1, x_2, \dots, x_n are the measured values of each angle parameter, Δx_n is the random error that conforms to the standard normal distribution and represents various errors that may occur when the airborne camera actually works. The calculation result of Eq. (23) is equivalent to the positioning error calculated by the space two-point distance formula, where $T_E^R = [x_r \ y_r \ z_r]$ is the real coordinate of the target in the ECEF coordinate frame and $T_E^D = [x_d \ y_d \ z_d]$ is the target point positioning result calculated in the simulation analysis.

$$d = \sqrt{(x_r - x_d)^2 + (y_r - y_d)^2 + (z_r - z_d)^2}. \quad (24)$$

In the simulation process, the parameters in Table 1 were taken as the real value, and the corresponding random error sequence was added to each parameter. The positioning error was calculated according to Eq. (16) and the circular probability error (CEP) was used as the

Table 1 Simulation experiment parameters of camera.

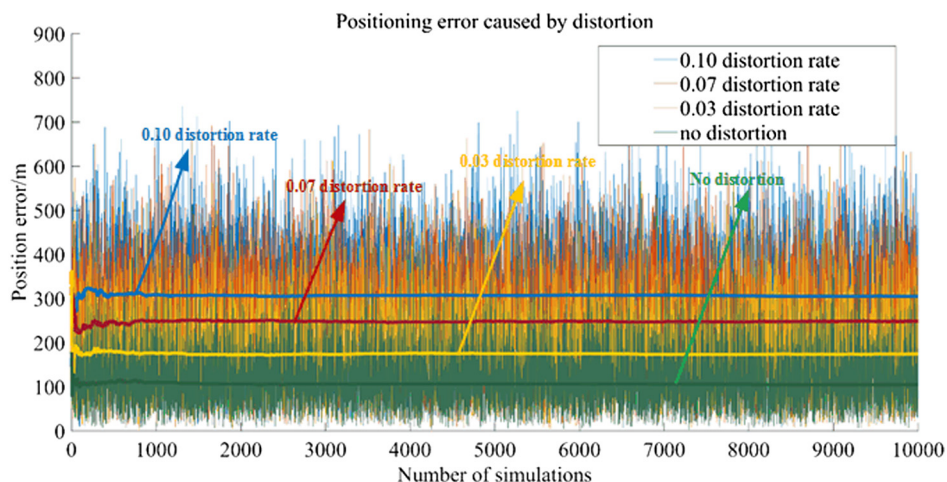
Error type		Real value	Error value (σ)
Camera position	Latitude (north)	35 deg	0.0001 deg
	Longitude (east)	110 deg	0.0001 deg
	Altitude (down)	7000 m	10 m
Camera attitude	Yaw	15 deg	0.05 deg
	Pitch	3 deg	0.01 deg
	Roll	0 deg	0.01 deg
Gimbal angle	Outer (roll)	78.2271 deg	0.006 deg
	Inner (pitch)	-2 deg	0.006 deg

evaluation index for the positioning accuracy. The camera's horizontal and vertical image pixel numbers are, respectively, 3840 and 3072, the single CCD pixel size is $8 \mu\text{m}$, the camera focal length is 1.5 m, and the shooting distance is 50 km.

In a simulation environment, assume that the target point is projected to the upper left corner of the CCD frame. The accuracy of the geolocation algorithm with and without distortion can be compared. Figure 7 shows the positioning error and the CEP for different distortion rates over 10,000 simulations. The fold line in the figure is the CEP of the corresponding distortion rate, and the ordinate is the positioning error value. It can be clearly seen that the positioning error increases with the increase in the distortion rate.

Figure 8 shows the effect of distortion on longitude and latitude errors, in the case in which the distortion rate is 0.04. It can be seen that the overall results of the longitude with distortion are 0.001 deg larger than those without distortion, and under the simulated shooting conditions shows in Table 1, the latitude positioning results have little effect. However, these results are not absolute. Image distortion does not have any effect on the latitude positioning error, which is related to the camera's own position and imaging angle. Depending on the camera's longitude, latitude, and imaging angle, image distortion will cause the positioning result to shift in a certain direction. This direction is not fixed, but it will eventually lead to positioning error.

In the simulation environment, the area where the target point is located is a flat area with an elevation standard deviation of 0 m. Therefore, there is no elevation positioning error, and the two-dimensional plane can be used to describe the positioning result by using the longitude and latitude. Figure 9 shows the positioning results of the target points obtained over 10,000

**Fig. 7** Schematic representation of positioning error caused by distortion.

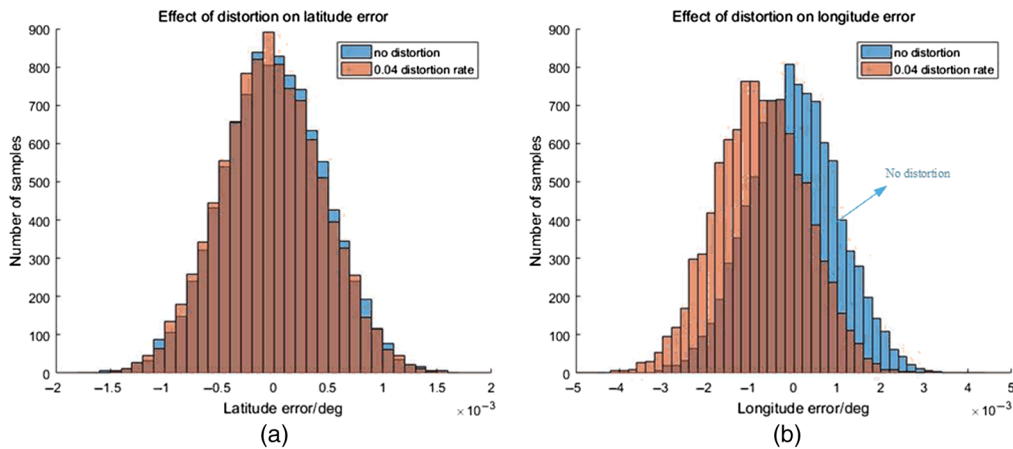


Fig. 8 Schematic representation of positioning error of longitude and latitude caused by distortion: (a) effect of distortion on longitude error and (b) effect of distortion on latitude error.

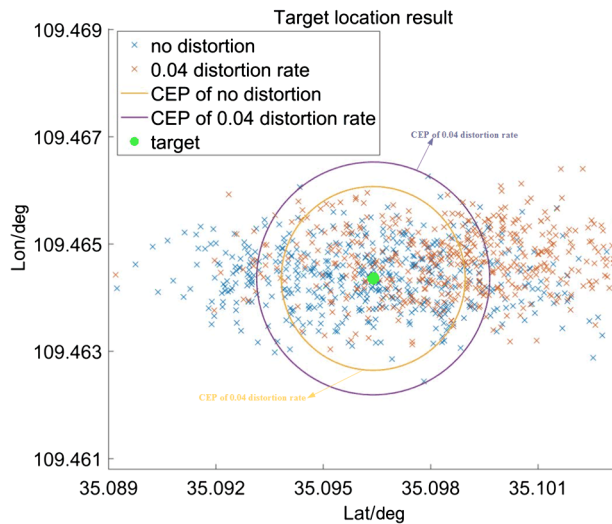


Fig. 9 Schematic representation of target location results with and without distortion.

simulations. It can be seen that image distortion causes the positioning results to shift relative to the real target position, and the accuracy of the geolocation algorithm is affected. The distribution of the target positioning results is described in detail, and it can be seen that the CEP with distortion is larger than that without distortion.

In summary, distortion has a significant impact on the accuracy of the geolocation algorithm. As the distortion rate increases, the error of the target positioning result also gradually increases.

4 Flight Experiment and Results

To prove the effectiveness of the distortion measurement and positioning error correction algorithm established in this paper, the images taken by the actual flight of airborne camera are used as the experimental data, and the appropriate target in the image is selected as the positioning object. The actual position of the target points is obtained by single-reference station differential global position system. Its positional accuracy can reach 0.2 m after processing and can be used as a standard value. Figure 10 presents a series of remote sensing images taken by an HLOAC. The camera operation overlap ratio was set to 20% when these images were captured.

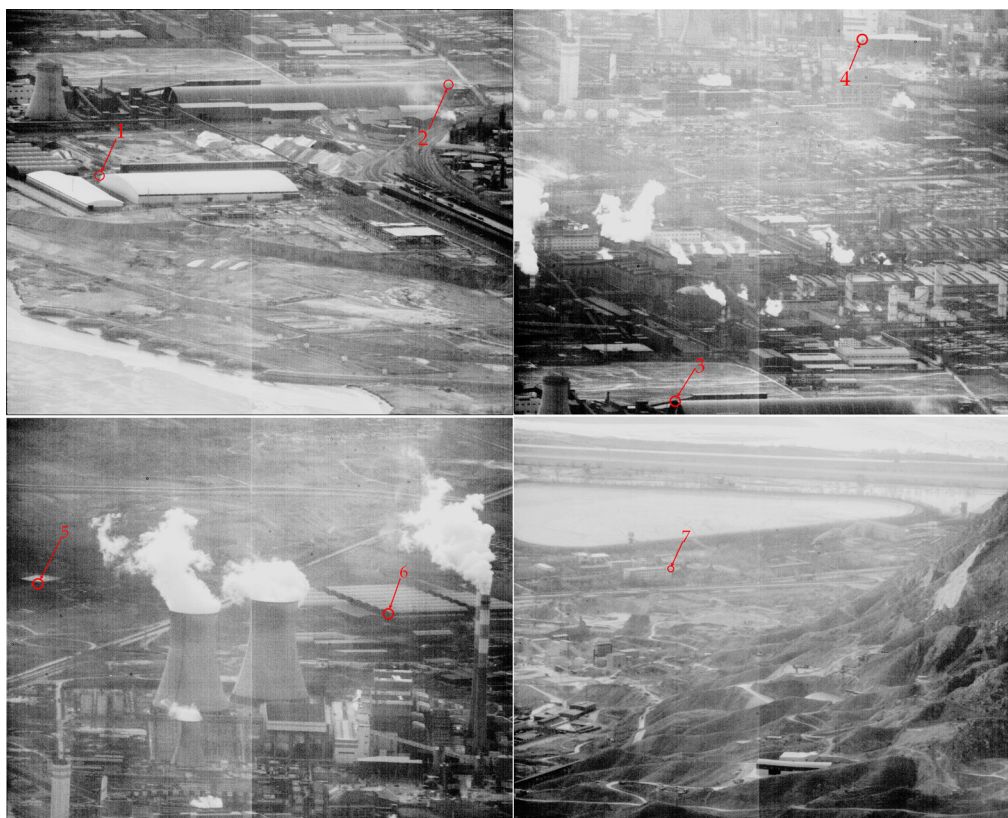


Fig. 10 Remote sensing images from the flight test.

Table 2 Distortion rate data provided by the laboratory.

Pixel position (j)	0	0.2	0.4	0.6	0.8	1
Distortion rate	0	0.0002	0.0005	0.0010	0.0018	0.003

The airborne camera used in the experiment was subjected to distortion measurement in the laboratory before the images were captured. The distortion rate data (the maximum distortion rate was 0.2%) given by the ground laboratory is shown in Table 2.

The distortion data measured by the laboratory does not consider the working environment of the camera. For comparison, using the distortion measurement algorithm established in this study, the distortion rate curve is plotted, as shown in Fig. 11. The ordinate is the distortion rate, and the abscissa is the position of the target projection point in the CCD coordinate frame. Taking the four consecutive images in Fig. 10 as the experimental data, according to the parameters in the annotation information on the current remote sensing images, the geolocation algorithm was used to locate the target points in the images, and the obtained results are shown in Tables 3 and 4. In the tables, A_1 , A_2 , B_1 , and B_2 are the overlapping targets required to calculate the distortion, which are located at the edge position of the second image, while O_1 , O_2 , and O_3 are the center points of the three images.

Table 5 shows the results of locating the target points using the geolocation algorithm in the case of ignoring the image distortion, recorded as situation 1. Table 6 shows the positioning results corrected based on the distortion rate provided by the laboratory, recorded as situation 2. Table 7 shows the positioning results corrected according to the distortion rate curve in Fig. 11, recorded as situation 3.

Figure 12 shows the change of the positioning errors in Tables 5–7, which can more clearly analyze the difference of positioning results in three different situations. Experimental remote

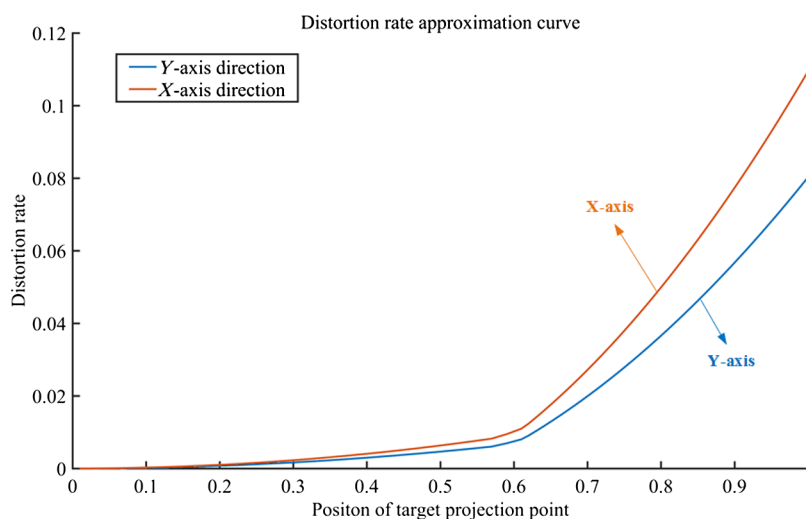


Fig. 11 Distortion rate curve of airborne camera.

Table 3 Data in flight experiment.

Target point	A1	B1	A2	B2
Projection position	(0,922)	(0,-922)	(0,-1536)	(0,1536)
Camera latitude/deg	35.935304	35.935422	35.935342	35.935342
Camera longitude/deg	110.868448	110.868344	110.868415	110.868415
Camera altitude/m	7532	7532	7532	7532
Aircraft yaw/deg	312.02	312.03	312.025	312.025
Aircraft pitch/deg	3.288	3.293	3.288	3.288
Aircraft roll/deg	0.273	0.272	0.275	0.275
Gimbal roll/deg	80.1800	81.2713	80.7310	80.7310
Gimbal pitch/deg	-5.32	-5.46	-5.39	-5.39
Target latitude/deg	35.625355	35.600871	35.625852	35.599606
Target longitude/deg	110.581725	110.551910	110.582508	110.558251

sensing images have larger imaging angles and a wider shooting range, and the positioning error of each pixel in the image is not uniform. Because the selected target points are distributed at different positions in the image, the distortion rate of each target is different, and the positioning errors caused by other error sources, such as altitude and atmospheric refraction, are also different. The positioning error of the image edges is usually larger, such as the error in target points 4 and 5, which is greater than that of the other points. Obviously, the positioning error of the geolocation algorithm is the largest when the distortion is ignored. In the target points used for the test, the minimum positioning error is also 160 m. The distortion correction can correct the positioning error caused by the distortion. In situation 2, the positioning error is only reduced by 10 m. This is because the distortion rate given by the laboratory is only the distortion of the optical system of the camera and ignores the image distortion caused by the imaging environment. As a result, the distortion rate is small, and the correction effect on the positioning error is also poor. The results of the positioning data, which are given in Table 7, are the best in the three cases. After calculating the image distortion rate using the algorithm given in this study, the positioning error caused by the image distortion is considerably corrected compared with situation 1, and the positioning accuracy is improved by 30%.

Table 4 Data of image center in flight experiment.

Target point	O1	O2	O3
Projection position	(0,0)	(0,0)	(0,0)
Camera latitude/deg	35.935304	35.935342	35.935422
Camera longitude/deg	110.868448	110.868415	110.868344
Camera altitude/m	7532	7532	7532
Aircraft yaw/deg	312.02	312.025	312.03
Aircraft pitch/deg	3.288	3.288	3.293
Aircraft roll/deg	0.273	0.275	0.272
Gimbal roll/deg	80.1800	80.7310	81.2713
Gimbal pitch/deg	-5.32	-5.39	-5.46
Target latitude/deg	35.632473	35.613364	35.592169
Target longitude/deg	110.588188	110.570460	110.551301

Table 5 Data of geolocation results.

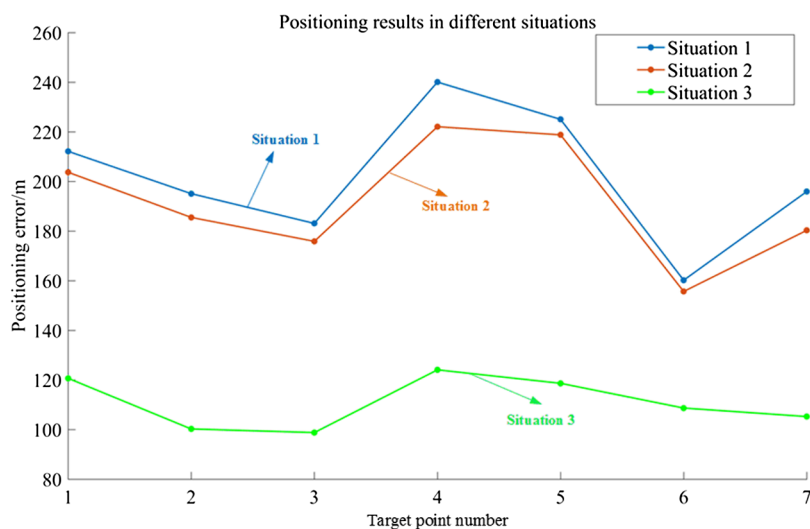
Target point	1	2	3	4	5	6	7
Projection position	(-1210,286)	(1430,984)	(-692,-1426)	(754,1318)	(-1656,292)	(996,56)	(-722,388)
Camera latitude/deg	35.935304	35.935304	35.935342	35.935342	35.935422	35.935422	35.935164
Camera longitude/deg	110.868448	110.868448	110.868415	110.868415	110.868344	110.868344	110.868571
Camera altitude/m	7532	7532	7532	7532	7532	7532	7532
Aircraft yaw/deg	312.02	312.02	312.025	312.025	312.03	312.03	312.018
Aircraft pitch/deg	3.288	3.288	3.293	3.293	3.293	3.293	3.281
Aircraft roll/deg	0.273	0.273	0.272	0.272	0.272	0.272	0.273
Gimbal roll/deg	80.1810	80.1810	80.7310	80.7310	81.2713	81.2713	79.0990
Gimbal pitch/deg	-5.31	-5.31	-5.32	-5.32	-5.329	-5.329	-5.29
Target location/deg	35.62892	35.62545	35.62449	35.60127	35.58756	35.59143	35.66086
	110.58849	110.57901	110.58325	110.55871	110.55276	110.54891	110.61604
Positioning result/deg	35.62800	35.62527	35.62643	35.59960	35.58638	35.59139	35.65948
	110.59038	110.57644	110.58374	110.55666	110.55418	110.54681	110.61776
Positioning error/m	212.1359	195.0860	183.0978	240.0249	225.0249	160.2060	195.9480

Table 6 Geolocation results after correction of distortion rate by laboratory.

Target point	1	2	3	4	5	6	7
Distortion rate (x)	0.0010	0.0015	0.0004	0.0005	0.0022	0.0007	0.00044
Distortion rate (y)	0.0002	0.0001	0.0026	0.0021	0.0002	0.00043	0.00025
Positioning result/deg	35.628078 110.590202	35.625300 110.576725	35.626241 110.583646	35.599748 110.556853	35.586566 110.553972	35.591416 110.546896	35.659671 110.617520
Positioning error/m	203.8065	185.5364	175.9105	222.1692	218.1984	155.3780	180.9873

Table 7 Geolocation results after correction of distortion rate curve.

Target point	1	2	3	4	5	6	7
Distortion rate (x)	0.0141	0.0368	0.0033	0.0039	0.0665	0.0068	0.0036
Distortion rate (y)	0.0006	0.0117	0.0631	0.0479	0.0007	0.0002	0.0012
Positioning result/deg	35.628385 110.589446	35.625321 110.577746	35.625433 110.583292	35.600393 110.557593	35.586900 110.553583	35.591428 110.547422	35.660130 110.616878
Positioning error/m	120.8465	100.2913	98.1057	124.2526	118.7379	108.6971	105.4002

**Fig. 12** Schematic representation of positioning error under different condition.

It can be seen that due to the working environment of HLOAC, image distortion caused by environmental factors such as atmospheric refraction and the earth's curvature has a great influence on the positioning result. In the flight experiment process, after correcting the CCD coordinates with the distortion rate, the positioning error could be reduced by about 50 to 100 m on the basis of 180 to 240 m, and the positioning accuracy was greatly improved. Correction using the proposed algorithm can effectively reduce positioning error caused by distortion.

5 Conclusions

This study aimed to address the issue of the positioning results for images captured by HLOAC being greatly affected by image distortion. Traditional camera distortion measurements are commonly performed in the laboratory, relying on standard reference materials such as grid plates, without taking into account image distortion caused by the complex working environment of aerial cameras. To solve this problem, a distortion measurement algorithm and corresponding coordinate correction algorithm are proposed. Based on the continuous image data captured by the airborne camera, the image distortion generated during flight imaging can be accurately estimated. Based on the principle of the target geolocation algorithm, the coordinate value of the target projection point can be corrected in the camera coordinate system to correct the positioning error caused by image distortion.

Simulation analysis shows that as the distortion rate increases, the positioning error increases. Owing to the large imaging angle and the wide imaging range of HLOAC, image distortion has a greater impact on its positioning results. In the case where the distortion rate is 0.03, the flying height of the aerial camera is 7000 m, and the imaging distance is 50 km, the positioning error caused by image distortion is more than 80 m. In this paper, the effectiveness of the algorithm is proved by actual flight test. The experimental data show that the algorithm can effectively reduce the positioning error caused by distortion. When the shooting distance is 50 km, the image edge positioning accuracy for the experimental camera can be improved from 200 to 100 m using the correction algorithm, which meets the requirements for practical engineering applications.

6 Appendix A: A Basic Target Geolocation Algorithm

The establishment of the ECEF coordinate frame requires an earth ellipsoid model, a series of earth parameters defined by the World Geodetic System-1984 Coordinate System is as follows:

Earth ellipsoid model:

$$\frac{x^2}{R_e^2} + \frac{y^2}{R_e^2} + \frac{z^2}{R_p^2} = 1. \quad (25)$$

First eccentricity of the earth ellipsoid:

$$e = \frac{\sqrt{R_e^2 - R_p^2}}{R_e}. \quad (26)$$

The prime vertical radius of curvature when latitude is ϕ :

$$R_n = \frac{R_e}{\sqrt{1 - e^2 \sin^2 \phi}}, \quad (27)$$

where $R_e = 6378137$ m is the semi-major axis and $R_p = 6356752$ m is the semi-minor axis.

As shown in Fig. 13, the origin of ECEF coordinate frame is at the geometric center of the earth, the X axis points to the intersection of the equator and the prime meridian, the Z axis points to the geographical north pole, and Y axis forms an orthogonal right-handed set. The position of a target in the ECEF coordinate frame and its geographical location information can be transformed into each other, which means latitude, longitude, and altitude (λ, ϕ, h) . Therefore, using the position information provided by the Position and Orientation System carried by the camera, the coordinates of the camera in the ECEF coordinate frame can be determined as shown in Eq. (28):

$$\begin{bmatrix} X_E \\ Y_E \\ Z_E \end{bmatrix} = \begin{bmatrix} (R_n + h) \cos \phi \cos \lambda \\ (R_n + h) \cos \phi \sin \lambda \\ (R_n(1 - e^2) + h) \sin \phi \end{bmatrix}. \quad (28)$$

The geographical location information can also be solved by ECEF coordinate values, which are usually calculated in an iterative manner, as shown in Eq. (29). Usually the north latitude and the east longitude are regarded as positive values.

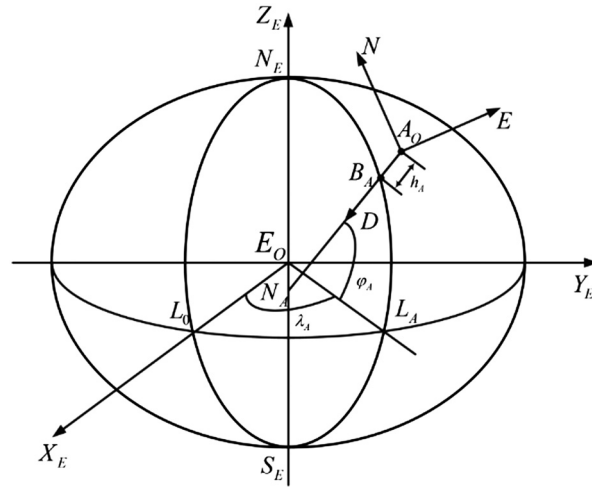


Fig. 13 Schematic representation of the ECEF coordinate and the NED coordinate.

$$\begin{cases} N_0 = R_e \\ h_0 = [(x_T)^2 + (y_T)^2 + (z_T)^2]^{1/2} - (R_e R_p)^{1/2} \\ \varphi_0 = \arctan \left\{ \frac{z_T [(1-e^2)N_0 + h_0]}{[(x_T)^2 + (y_T)^2]^{1/2} (N_0 + h_0)} \right\} \end{cases}, \quad \begin{cases} N_i = \frac{R_E}{(1-e^2 \sin^2 \varphi_{i-1})^{1/2}} \\ h_i = \frac{[(x_T)^2 + (y_T)^2]^{1/2}}{\cos \varphi_{i-1}} - N_{i-1} \\ \varphi_i = \arctan \left\{ \frac{z_T [(1-e^2)N_{i-1} + h_{i-1}]}{[(x_T)^2 + (y_T)^2]^{1/2} (N_{i-1} + h_{i-1})} \right\} \end{cases} \quad (29)$$

Equation (29) can be used to calculate the latitude and altitude of the target, and the longitude of the target can be obtained by Eq. (30):

$$\lambda_0 = \arctan \left(\frac{y_T}{x_T} \right), \quad \lambda = \begin{cases} \lambda_0 & x_T > 0 \\ \lambda_0 + \pi & x_T < 0, \lambda_0 < 0 \\ \lambda_0 - \pi & x_T < 0, \lambda_0 > 0 \end{cases} \quad (30)$$

The geographical coordinate frame takes the position of airborne camera as the origin, it also names the NED coordinate frame, the *N* and *E* axes point to real north and real east, and the *D* axis points to geocentric along the normal line of the earth ellipsoid. Equation (31) is the transformation matrix between the ECEF and the NED coordinate frames.

$$C_{ECEF}^{NED} = \begin{bmatrix} 1 & 0 & 0 & 0 \\ 0 & 1 & 0 & 0 \\ 0 & 0 & 1 & R_n + h \\ 0 & 0 & 0 & 1 \end{bmatrix} \times \begin{bmatrix} -\sin \varphi & 0 & \cos \varphi & 0 \\ 0 & 1 & 0 & 0 \\ -\cos \varphi & 0 & -\sin \varphi & 0 \\ 0 & 0 & 0 & 1 \end{bmatrix} \times \begin{bmatrix} \cos \lambda & \sin \lambda & 0 & 0 \\ -\sin \lambda & \cos \lambda & 0 & 0 \\ 0 & 0 & 1 & 0 \\ 0 & 0 & 0 & 1 \end{bmatrix} \\ \times \begin{bmatrix} 1 & 0 & 0 & 0 \\ 0 & 1 & 0 & 0 \\ 0 & 0 & 1 & R_n e^2 \sin \varphi \\ 0 & 0 & 0 & 1 \end{bmatrix} \quad (31)$$

The A coordinate frame takes the center of the camera optical system as its origin, the *X* axis is pointing to the nose of the aircraft, the *Y* axis is pointing to the right wing, and the *Z* axis down forms an orthogonal right-handed set.

The origin of the C coordinate frame is consistent with the A coordinate frame, the axis is the LOS of the imaging system, and the internal and external frame angles (θ_{pitch} and θ_{roll}) exist when the camera is working. Figure 14 shows the relationships between the above coordinate frames, and the transformation matrices between them are as follows:

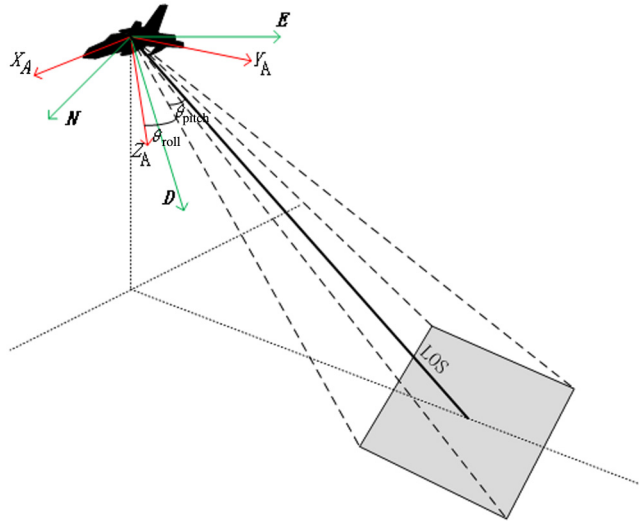


Fig. 14 Schematic representation of the NED coordinate and the A coordinate and C coordinate.

$$C_{NED}^A = \begin{bmatrix} 1 & 0 & 0 & 0 \\ 0 & \cos \varphi & \sin \varphi & 0 \\ 0 & -\sin \varphi & -\cos \varphi & 0 \\ 0 & 0 & 0 & 1 \end{bmatrix} \times \begin{bmatrix} \cos \theta & 0 & -\sin \theta & 0 \\ 0 & 1 & 0 & 0 \\ \sin \theta & 0 & \cos \theta & 0 \\ 0 & 0 & 0 & 1 \end{bmatrix} \times \begin{bmatrix} \cos \psi & \sin \psi & 0 & 0 \\ -\sin \psi & \cos \psi & 0 & 0 \\ 0 & 0 & 1 & 0 \\ 0 & 0 & 0 & 1 \end{bmatrix}, \quad (32)$$

$$C_A^C = \begin{bmatrix} \cos \theta_{pitch} & 0 & -\sin \theta_{pitch} & 0 \\ 0 & 1 & 0 & 0 \\ \sin \theta_{pitch} & 0 & \cos \theta_{pitch} & 0 \\ 0 & 0 & 0 & 1 \end{bmatrix} \times \begin{bmatrix} 1 & 0 & 0 & 0 \\ 0 & \cos \theta_{roll} & \sin \theta_{roll} & 0 \\ 0 & -\sin \theta_{roll} & \cos \theta_{roll} & 0 \\ 0 & 0 & 0 & 1 \end{bmatrix}. \quad (33)$$

If the altitude of the target is h_T , the earth ellipsoid equation at that point is as shown in Eq. (34):

$$\frac{x_T^2}{(R_e + h_T)^2} + \frac{y_T^2}{(R_e + h_T)^2} + \frac{z_T^2}{(R_e + h_T) \times (1 - e^2)^{1/2}} = 1. \quad (34)$$

The geographical location information of the target point can be obtained by using the above transformation matrix and the linear equation described in Sec. 2.1.2.

Acknowledgments

This research was funded by the Major State Basic Research Development Program of China, Grant No. 2016YFC0803000. The authors declare no conflict of interest.

References

1. E. J. Stich, "Geo-pointing and threat location techniques for airborne border surveillance," in *IEEE Int. Conf. Technol. for Homeland Secur.*, pp. 136–140 (2013).
2. C. Qiao, Y. Ding, and Y. Xu, "Ground target geolocation based on digital elevation model for airborne wide-area reconnaissance system," *J. Appl. Remote Sens.* **12**(1), 016004 (2018).

3. C. Qiao et al., "Ground target geo-location using imaging aerial camera with large inclined angles," *Opt. Precis. Eng.* **25**, 1714–1726 (2017).
4. K. J. Held and B. H. Robinson, "TIER II plus airborne EO sensor LOS control and image geolocation," in *Proc. Aerosp. Conf.*, pp. 377–405 (1997).
5. S. Sohn et al., "Vision-based real-time target localization for single-antenna GPS-guided UAV," *IEEE Trans. Aerosp. Electron. Syst.* **44**(4), 1391–1401 (2008).
6. C. Sun et al., "Backscanning step and stare imaging system with high frame rate and wide coverage," *Appl. Opt.* **54**, 4960–4965 (2015).
7. H. Li et al., "Metadata-assisted global motion estimation for medium-altitude unmanned aerial vehicle video applications," *Remote Sens.* **7**(10), 12606–12634 (2015).
8. J. Wu et al., "A three-dimensional localization method for multistatic SAR based on numerical range-Doppler algorithm and entropy minimization," *Remote Sens.* **9**(5), 470 (2017).
9. S. Lee, T. E. Kim, and J. Choi, "Correction of radial distortion using a planar checkerboard pattern and its image," in *Int. Conf. Consum. Electron.* (2009).
10. H. Cui et al., "Image geometric correction based on distortion ratio," *J. Appl. Opt.* **27**(3), 183–186 (2006).
11. X. Xu et al., "Trend and development actuality of the real-time transmission airborne reconnaissance camera," *OME Inf.* **27**, 38–43 (2010).
12. X. Wang, J. Liu, and Q. Zhou, "Real-time multi-target localization from unmanned aerial vehicles," *Sensors* **17**, 33 (2017).
13. C. Liu et al., "A novel system for correction of relative angular displacement between airborne platform and UAV in target localization," *Sensors* **17**, 510 (2017).
14. L. Tan et al., "Error analysis of target automatic positioning for airborne photo-electric measuring device," *Opt. Precis. Eng.* **21**, 3133–3140 (2013).
15. G. Bai et al., "Two-UAV intersection localization system based on the airborne optoelectronic platform," *Sensors* **17**, 98 (2017).
16. W. Lee, H. Bang, and H. Leeghim, "Cooperative localization between small UAVs using a combination of heterogeneous sensors," *Aerosp. Sci. Technol.* **27**, 105–111 (2013).
17. H. Pan, C. Tao, and Z. Zou, "Precise georeferencing using the rigorous sensor model and rational function model for ZiYuan-3 strip scenes with minimum control," *ISPRS J. Photogramm. Remote Sens.* **119**(Suppl. C), 259–266 (2016).
18. S. Lee, S. Lee, and J. Choi, "Correction of radial distortion using a planar checkerboard pattern and its image," *IEEE Trans. Consum. Electron.* **55**(1), 27–33 (2009).
19. C. Su et al., "Distortion correction for images in planar metrology," *Opt. Precis. Eng.* **19**(1), 161–167 (2011).
20. S. R. M. Ahouandjinou, E. C. Ezin, and C. Motamed, "An approach to correcting image distortion by self-calibration stereoscopic scene from multiple views," in *Eighth Int. Conf. Signal Image Technol. and Internet Based Syst.*, IEEE, pp. 389–394 (2012).
21. S. Wang, S. Song, and X. Shi, "An improved adaptive correction method for camera distortion," in *Proc. 33rd Chin. Control Conf.* (2014).
22. G. Yao, K. Deng, and L. Zhang, "Robust perspective invariant quasidense matching across large oblique images," *J. Electron. Imaging* **23**(4), 043005 (2014).
23. Q. Zhou et al., "Automatic correction of geometric distortion in aerial zoom squint imaging," *Opt. Precis. Eng.* **23**, 2927–2942 (2015).
24. X. Tang et al., "Inner FoV stitching of spaceborne TDI CCD images based on sensor geometry and projection plane in object space," *Remote Sens.* **6**, 6386–6406 (2014).
25. N. Merkle et al., "Exploiting deep matching and SAR data for the geo-localization accuracy improvement of optical satellite images," *Remote Sens.* **9**, 586 (2017).

Yiming Cai is a PhD student at the University of Chinese Academy of Sciences. He got his BS degree in mechanical engineering and automation in 2016. His current research interests include stable imaging, target tracking, and geolocation technology of airborne cameras.

Yalin Ding is a senior researcher at Changchun Institute of Optics, Fine Mechanics, and Physics, Chinese Academy of Sciences. His current research interests include airborne camera systems design and airborne photoelectric sensor imaging and measurement systems.

Jihong Xiu is a researcher at Changchun Institute of Optics, Fine Mechanics, and Physics, Chinese Academy of Sciences. He received his PhD from the University of the Chinese Academy of Sciences in 2005. Her current research interests include signal processing algorithm design and aerial camera image processing and analysis.

Hongwen Zhang is a researcher at Changchun Institute of Optics, Fine Mechanics, and Physics, Chinese Academy of Sciences. His research direction is the mechanical structure design of airborne cameras

Chuan Qiao is a doctor at Beijing Institute of Control Engineering. He received his PhD from the University of Chinese Academy of Sciences. His current research interests include geolocation and line-of-sight stabilization techniques.

Qihui Li is a master student at the University of Chinese Academy of Sciences. His research direction is aerial camera dimming and focusing technology.